A Numerical Study for the Three-Dimensional Fluid Flow Past Tube Banks and Comparison with PIV Experimental Data

Man Yeong Ha*, Seung-Hyeon Kim, Kyung Chun Kim
School of Mechanical Engineering, Pusan National University, Pusan 609-735, Korea
Young Chul Son
LG Electronics, Digital Appliance Co., 391-2, Gaeumjeong-dong, Changwon City, Gyeongnam 641-711, Korea

The analysis for the three-dimensional fluid flow past tube banks arranged in equilateral-triangular form at Re_{max}=4,000 is carried out using a large eddy simulation technique. The governing equations for the mass and momentum conservation are discretized using the finite volume method. Parallel computational techniques using MPI (Message Passing Interface) are implemented in the present computer code. The computation time decreases linearly proportional to the number of used CPUs in the present parallel computation. We obtained the time-averaged streamwise and cross-streamwise velocities and turbulent intensities. The present numerical results are compared with the PIV experimental data and agree generally well with the experimental data.

Key Words: Tube Bundle, Fluid Flow, LES, Parallel Computing

1. Introduction

The phenomenon of flow separation, bluff body wake and prediction of heat transfer from a single cylinder (Ahmad, 1996; Braza et al., 1986; Karniadakis and Triantafyllou, 1992; Kravchenko and Moin, 2000; Mittal and Balachandar, 1994, 1995; Ryu et al., 2003; Tamura and Ohta, 1990; Thompson et al., 1996; Williamson 1996a, 1996b; Zhang and Dalton, 1998) and tube bundle (Barsamian and Hassan, 1997; Beale and Spalding, 1999; Krishne et al., 1998; Wang et al., 2000; Watterson et al., 1999; Wilson and Bassiouny, 2000; Yoo et al., 2002) have long been intensely studied because of its fundamental significance in ctical importance in aerodynamic and heat transfer applications. For example, complex wakes are found behind tube bundles in heat exchangers, fuel and control guide rods in nuclear reactors, piers and bridge pilings, oil and gas pipelines, cooling-tower arrays, suspension bridges and high-rise buildings. These complex wakes are usually formed by the interactions of a number of simple wakes generated by individual structures. Richer phenomena ranging from steady to unsteady and two-dimensional to three-dimensional cases are exhibited in fluid flow and heat transfer past cylinders. Many numerical simulations for the fluid flow and heat transfer past tube bundles have been restricted to two-dimensional and steady state cases for the laminar (Wang et al., 2000) and turbulent (Watterson et al., 1999; Wilson and Bassiouny, 2000a, 2000b) flows. However, the flow and thermal fields never become steady and two-dimensional as the Reynolds number increases. So there are some discrepancies between unsteady two- and

* Corresponding Author,
E-mail: myha@hyowon.pusan.ac.kr
TEL: +82-51-510-2440; **FAX**: +82-51-512-9835
School of Mechanical Engineering, Pusan National University, Pusan 609-735, Korea. (Manuscript **Received** November 14, 2003; **Revised** September 14, 2004)

three-dimensional simulations for the case past a single cylinder and tube bundles (Barsamian and Hassan, 1997; Krishne Gowda et al., 1998). Many studies performed unsteady 2D simulations of flow past tube bundles using different techniques of finite difference, finite volume and finite element methods for a wide range of the Reynolds numbers. These studies investigate the generation and evolution of vortical structures, wakes interactions, and their effects on the drag, heat transfer, flow-induced vibration and noise problems, which are caused by the flow past circular cylinders. However, there are little studies to solve the three-dimensional and time-dependent fluid flow (Beale and Spalding, 1999) and heat transfer past a bank of tubes numerically and to compare their numerical results with PIV experimental data.

In the present study, we studied the unsteady and three-dimensional fluid flow past the bank of tubes in detail by using the finite volume method and parallel computing technique based on MPI (Message Passing Interface). The tube rows of a bank in the present study are staggered in the flow direction and arranged in the equilateral-triangular form. $Re_{D,\max}$=4,000 is used in the present calculation where $Re_{D,\max}$ is based on the maximum velocity occurring within the tube bank. $Re_{D,\max}$= 4,000 is the Reynolds number which we have met frequently in the design of a heat exchanger. The present computational results are compared with measured data obtained from PIV experiments. The computed results generally well represent the PIV experimental data.

2. Numerical Methodology

For the incompressible, constant property flow considered here, the basic governing equations for the large eddy evolution for the flow past a staggered tube bank are the grid-filtered Navier-Stokes and continuity equations.

$$\frac{\partial \bar{u}_i}{\partial t}+\frac{\partial \bar{u}_i\bar{u}_j}{\partial x_j}=-\frac{\partial \bar{p}}{\partial x_i}+\frac{1}{\mathrm{Re}}\frac{\partial^2 \bar{u}_i}{\partial x_j\partial x_j}-\frac{\partial \tau_{ij}}{\partial x_j} \quad (1)$$

$$\frac{\partial \bar{u}_i}{\partial x_i}=0 \quad (2)$$

where overbar denotes the large (or resolved) scale obtained from grid-filtering. The box-filter is used in the present study. The effect of the subgrid scale motion on the dynamics of the resolved velocity is described by the subgrid scale stress tensor defined as

$$\tau_{ij}=\bar{u}_i\bar{u}_j-\bar{u}_i\bar{u}_j \quad (3)$$

which must be modeled in terms of the resolved scale velocity, $\bar{u}_i$, in order to close Eq. (1). In the present study, we used Smagorinsky model to represent the anisotropic part of the subgrid scale stress tensor defined as

$$\tau_{ij}=-(C_S\Delta)^2(2\bar{S}_{lm}\bar{S}_{lm})^{1/2}\bar{S}_{ij}+\frac{1}{3}\tau_{kk}\delta_{ij} \quad (4)$$

where C_S is Smagorinsky coefficient. Different values for C_s have been proposed. For homogeneous isotropic turbulence with cutoff in the inertial subrange and Δ equal to the grid size, $C_s\approx 0.23$ is used commonly. However, in the present study with the mean shear, C_s=0.18 is used. (Mason and Callen, 1986). Δ in Eq. (4) is the filter width defined as (Germano et al., 1991)

$$\Delta=(\Delta_1\Delta_2\Delta_3)^{1/3} \quad (5)$$

where Δ_i represents the grid spacing in the i-th direction. $\bar{S}_{ij}$ in Eq. (4) is the large scale strain tensor defined as

$$\bar{S}_{ij}=\frac{1}{2}\left(\frac{\partial \bar{u}_i}{\partial x_j}+\frac{\partial \bar{u}_{ij}}{\partial x_i}\right) \quad (6)$$

The dimensionless variables in the above equations are defined as

$$t=\frac{U_{in}t^*}{D},\ x_i=\frac{x_i^*}{D},\ u_i=\frac{u_i^*}{U_{in}},\ p=\frac{p^*}{\rho U_{in}^2} \quad (7)$$

In the above equations, U_{in}, D and ρ represent the inlet velocity, the diameter of cylinder and the density. The superscript * in Eq. (7) represents the dimensional variables. u_i, p, t and x_i denote the dimensionless velocity, pressure, time and coordinates, respectively. The above non-dimensionlization results in one dimensionless parameter: $Re=U_{in}D/v$ where v is the kinematic viscosity.

Table 1 Specification of PC cluster

Hardware	CPU : Dual Intel P-III 550 MHz Memory : 512 MB SDRAM LAN-Card : Universal, 64/32 bit, 66/33 MHz, Myrinet-LAN Switch : 16-port Myrinet-LAN switch
Software	OS : Alzza Linux 6.1 Parallel Application : MPICH-1.2.1
Processors used	24 processors

The governing Eqs. (1) and (2) are defined in the generalized coordinate system to consider the complex geometry of the present problem. The finite volume method under the non-staggered grid system is used for the discretization of the governing equations. We used the modified QUICK scheme (Ghosh Roychowdhury et al., 1999) for integration of the convection terms and second-order central difference scheme for the other terms, respectively. The SIMPLE algorithm is used for the velocity-pressure segregation and time integration (Patankar, 1980).

The developed computer code is parallelized based on the MPI (Message Passing Interface) to increase the computational speed. Table 1 shows the specification of the computer hardware and MPI libraries used for the parallelization of the developed code. We used the virtual topology method in the MPI programming technique. In the virtual topology method, the processors used in the parallel computation are arranged virtually in two- or three-dimensional way and have their own independent coordinates. Using this method, we can make the programming for the data exchange between the processors during the parallel computing easier and manage flexibly the change in the number of processors used in the parallel computing. The two-dimensional virtual topology method is used in the present study. The number of processors used is 12 in the streamwise direction and 2 in the cross-streamwise direction, respectively, to consider the larger length of the computational domain in the streamwise direction, compared to that in the cross-streamwise direction. A same number of grid point is allocated to each processor. We also define a ghost point using an extra array at the interface of processors. The ghost point is used as a place to store the information when we exchange the computed results at the interface between the adjacent processors. In order to perform highly fast and efficient calculation in the parallel computation, the computation time allocated to each processor should be equally distributed and the boundary values between the adjacent processors should be treated very carefully. In the present study, we exchanged frequently the mass flux and contra-variant velocities at the interface between adjacent processors while we carried out the computation in the matrix solver loop of our computer code and obtained the continuous values for velocities and pressure at the interface. The speed-up ratio of the present parallel computing algorithm is tested by running our computer code for the case of fluid flow in the rectangular cavity. The computational time using multi-processors is compared with that using a single processor, resulting in a decreasing computational time, which is almost linearly proportional to the number of processors (Kim, 2002).

3. Experimental Methodology

3.1 Experimental apparatus and conditions

The schematic diagram of the experimental apparatus is shown in Fig. 1. Measurements were made in an open circuit low speed wind tunnel. The test section has a dimension of 800 mm in width, 300 mm in height and 2,000 mm in length. It is made of glass plates to minimize the reflection of the images. Air can be delivered to the wind tunnel by a 2205 W (3 Hp) variable-speed centrifugal fan and entered to the test section through a settling chamber followed by a 2.67 : 1 contraction nozzle. The uniformity of mean velocity profile of the flow at the nozzle exit is less than 0.8% except the area near the test section walls within 10 mm distance. The free stream turbulence level at the test section is less than 1%.

Data were taken at a fixed free stream velocity, $U=1.24$ m/s, so that the corresponding Reynolds

number based on the maximum velocity and the tube diameter was set to be 4,000 which is the range widely used in a commercial heat exchanger. Figure 2(a) presents the configuration of the staggered tube bundle model. There are five rows of tubes and each row has four cylinders. Half-cut dummy cylinders are attached on the top and bottom plates to reproduce real flow conditions

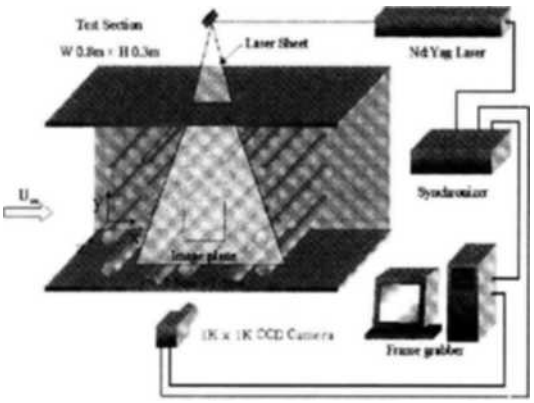

Fig. 1 A schematic diagram of experimental setup

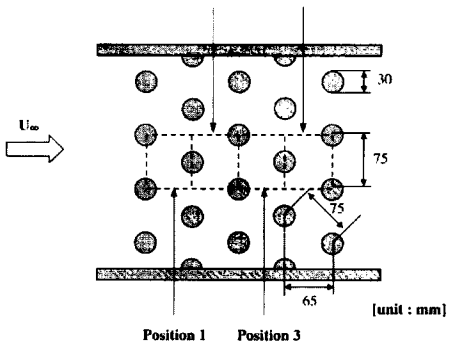

(a) Physical domain

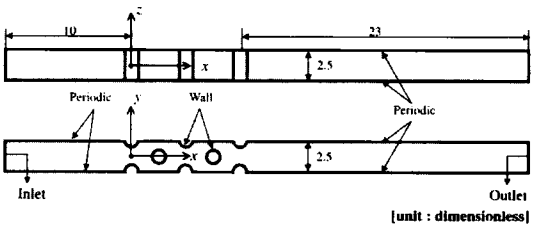

(b) Computational domain

Fig. 2 (a) Physical domain to represent flow configuration, positions of image plane and coordinate system and (b) computational domain used to reproduce the PIV experiment

at the second and fourth rows of the tube bank. We have used 30 mm-diameter plexiglass tubes for the cylinders. Hence the aspect ratio, 1/26.7, seems to be enough to consider that the flow provides two-dimensionality. The arrangement of tubes is set to be a regular triangle form as the standard case. The longitudinal pitch (distance between two next rows) is 65 mm (75 cos 30°) and the transverse pitch (distance between two next columns) is 75 mm. As can be seen in Fig. 2(a), we denote position numbers to the four fields of view, which are representative flow areas between first to fifth rows.

3.2 PIV system and measurement method

The used digital PIV system consists of a 250 mJ/pulse Nd : Yag laser, an 1 K by 1 K high resolution CCD Camera (TSI, PIVCAM 10-15), a synchronizer (TSI 610032), a frame grabber (TSI 610066) and a personal computer to control the system. A Laskin nozzle was used to produce olive oil aerosol whose nominal diameter was 2 microns.

The field of view has a dimension of 75 mm by 75 mm. Since the longitudinal pitch is 65 mm, the captured image includes additional flow area beyond center to center of tubes as shown in Fig. 1. The velocity vectors were measured by two frame cross-correlation method and the interrogation window size was 24×24 pixels. With a 50% overlap allowed, we obtained 6,724 velocity vectors with 0.9 mm spatial resolution. TSI's Insight-NT was used only for taking images and timing control. All other post processings were performed using PIV ACE V1.0 which was developed in our laboratory (Yoon, 2000). The program includes a sub-pixel searching algorithm and a multiple-validation technique to reduce spurious vectors. In-situ compensation of image distortion is also available, so that the measured velocities are within 1% error bound. More detailed information about the PIV experiments is described in (Park, 2001).

4. Results and Discussion

For the purpose of code validation, the flow

past a single cylinder at Re=3900 is tested. The number of grid points is 386×122×40 in the x, y and z directions, respectively, giving the total grid points of 1,883,680. The minimum spacing of grid used is 0.0055 (0.55% of cylinder diameter), which is the distance to the next grid point from the cylinder wall. The present computed results for the time-averaged streamwise velocity along the centerline and time-averaged streamwise velocities along the cross-streamwise direction at different streamwise locations represent generally well PIV data (Lourenco and Shih 2000; Yoon, 2000) and DNS data (Kravchenko and Moin, 2000), as shown in Figs. 3 and 4. The present computed results for the time-averaged cross-streamwise velocity along the cross-streamwise direction at different streamwise locations also represent generally well PIV data (Lourenco and Shih, 2000; Yoon, 2000) and DNS data (Kravchenko and Moin, 2000), as shown by Kim (2002).

After the successful benchmark test, we investigated the flow past a bank of tubes for the geometry used in the PIV experiment (Park, 2001), as shown in Fig. 2(a). Figure 2(b) shows the computational domain used in the present calculation to reproduce the PIV experiment. The coordinate system is also defined in Fig. 2(b). The distances from the center of tubes in the first row to the inlet and from the center of tubes in the fifth row to the outlet are 10 and 23, respectively, which are 10 and 23 times longer than the cylinder diameter. The dimensionless length used in the spanwise direction is 2.5. The boundary conditions used in the present calculation are the inflow and outflow conditions at the inlet and outlet, periodic conditions in the cross-streamwise and spanwise directions and no-slip condition on the cylinder wall, as shown in Fig. 2(b). The number of grid points used in the full computational domain is 1,010×110×20 in the x, y and z directions, respectively, giving the total grid points of 2,222,000. Twenty four processors are used for the parallel computation. The time-averaged streamlines, velocities and Reynolds stress obtained from the present calculation

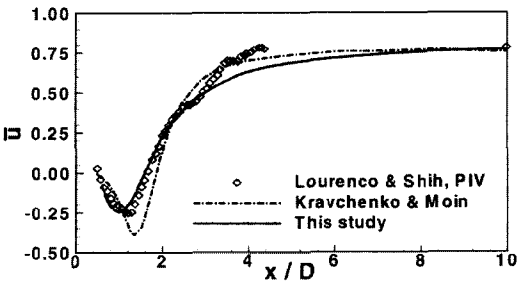

Fig. 3 Comparison of time-averaged streamwise velocity along the centerline for the flow past a single cylinder with PIV and DNS data

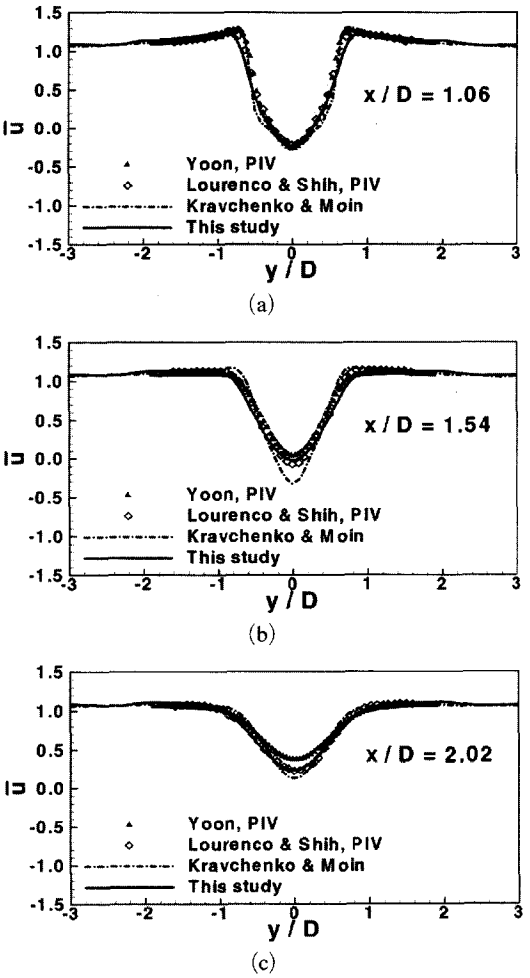

Fig. 4 Comparison of time-averaged streamwise velocity along the cross-streamwise direction at different streamwise locations for the flow past a single cylinder with PIV and DNS data

are compared with those obtained form the PIV experiment.

The time-averaged values are obtained by time-averaging the instantaneous values obtained during 200 dimensionless time and compared with the time-averaged PIV data. Figure 5 shows the time-averaged streamlines at different positions of 1~4. The streamlines obtained from the present calculation and PIV experiment are shown in the left and right sides of Figs. 5(a) ~ (d), respectively. Although we observed asymmetric flow characteristics in the instantaneous velocity fields, the time-averaged flow shows a perfect symmetric pattern. It means that the unsteady nature of the complex wake in the tube bundle must be an ergodic process. The distribution of streamlines obtained from the present calculation represents generally well those from the PIV experiment. Table 2 shows the length of recirculation region, L_F, in the wake obtained from both present calculation and PIV experiment. Here L_F is defined as a length from the rear stagnation point of tubes to the end of recirculation bubble where the time-averaged stramwise velocity $\bar{u}$ along the centerline in the wake changes from the negative or positive values to a zero value. As shown in Table 2, L_F obtained from the present calculation is slightly larger than that from PIV experiment. We think that this difference occurs because the present calculation does not predict completely the efflux of small-scale vortices formed on the surface of tubes and their disturbance to the recirculating flow in the wake. Another possible reason is that the experiment has performed with relatively high free stream turbulence, which usually shortens the recirculating region for the case of single circular cylinder wake flow. The difference between the present calculation and PIV experiment in the prediction of L_F may be improved by increasing the number of grid points used, compared to the present 2,222,000 grid points. The flow pattern in position 1 is generally similar to the flow past a single cylinder, resulting in $L_F=1.18D$. The main flow is accelerated and disturbed while it passes the first row of tube bank, due to the presence of tubes and wake.

Table 2 L_F at different positions of 1, 2, 3 and 4

	P1	P2	P3	P4
Experiment	1.05D	0.91D	0.72D	0.7D
Calculation (% Error)	1.18D (12.7%)	1.11D (21.6%)	0.89D (23.7%)	0. 79D (13.1%)

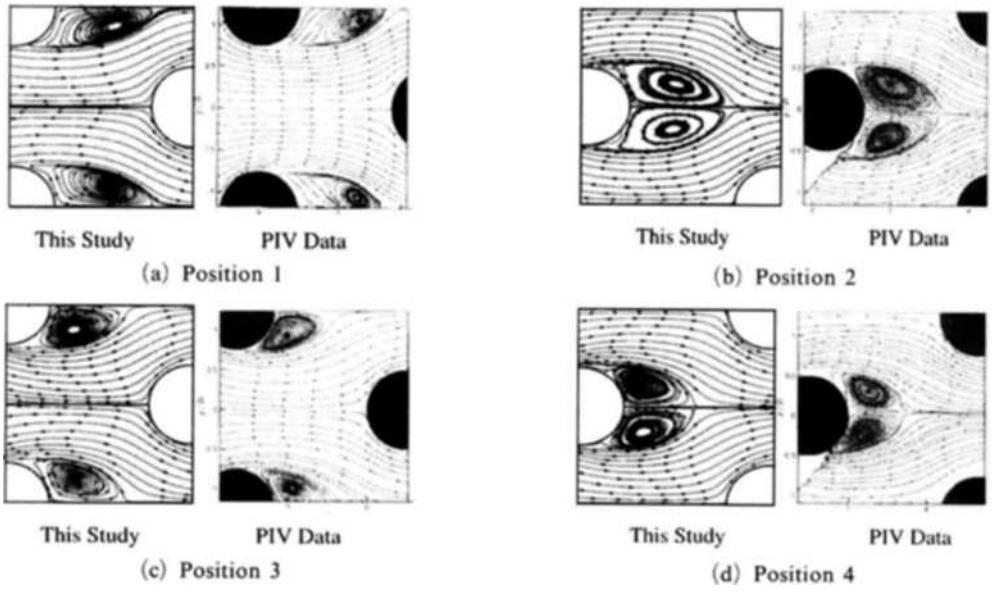

Fig. 5 Comparison of time-averaged streamlines obtained from the present calculation with PIV experiment

Thus, the shear layer in the second row of tube bank is disturbed and vortex efflux from the tube surfaces occurs in the more upstream region, resulting in shorter length of calculated recirculation region in positions 2 (L_F=1.11D) than that in position 1 (L_F=1.18D). L_F becomes shorter while the flow passes through the third and fourth row of tube bank, resulting in L_F= 0.89D in position 3 and L_F=0.79D in position 4. There are two reasons to explain the changes in the formation length of the separation bubble. One is that the accelerated jet-like flow produces much higher shear thickness of the separated shear layer, so that the bubble size could be reduced. The other reason can be thought that the increased free stream turbulence at the upstream region in the presence of tube bundles promotes boundary layer transition at the cylinder wall and enhances mixing in the near wake region.

Figures 6 and 7 show the distribution of time-averaged streamwise velocity ($\bar{u}$) and cross-streamwise velocity ($\bar{v}$) along the cross-streamwise direction (y) at different locations in the streamwise direction (x). The solid line and

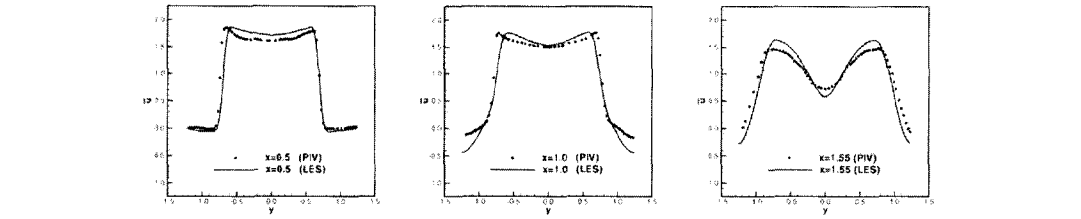

(a) Position 1

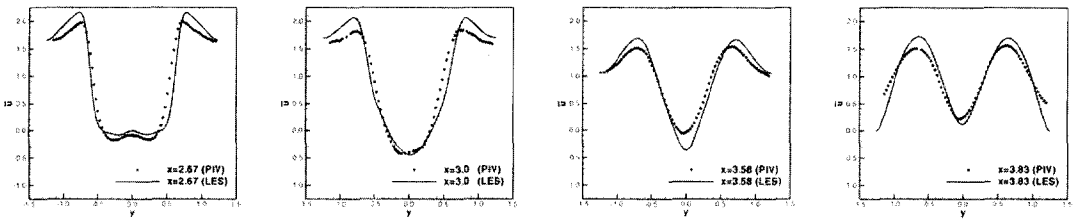

(b) Position 2

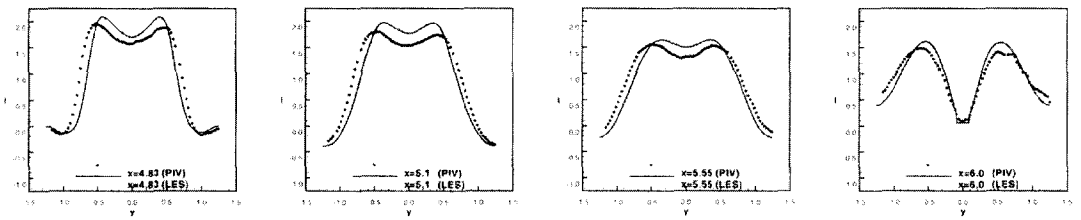

(c) Position 3

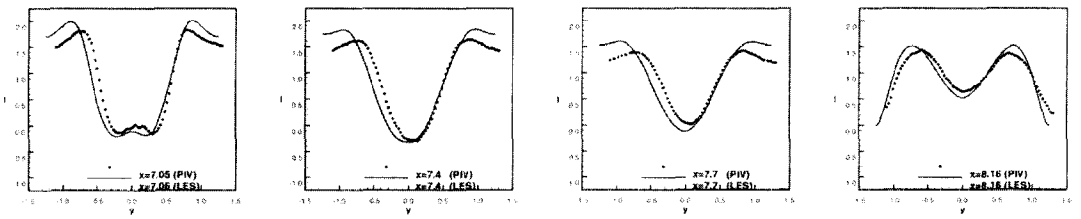

(d) Position 4

Fig. 6 Comparison of time-averaged streamwise velocity obtained from the present calculation with PIV experiment: (-) this study, (▪) PIV experiment

square symbol in these figures represent the LES calculated and PIV experimental results, respectively. In the region of position 1, the velocities of $\bar{u}$ and $\bar{v}$ have a profile of plug flow at $x=0.5$ and 1.0. At $x=1.55$ in front of the cylinder at the second row, the flow changes suddenly its profile to jet-like mode. At $x=2.67$ and 3.0 in the position 2, the velocities show the pattern corresponding to the wake flow behind the cylinders in the second row, resulting in a slightly modified "U" shape at $x=2.67$ and "V" shape at $x=3.0$ for the time-averaged streamwise velocity with small magnitude of time-averaged cross-streamwise velocities. At $x=3.58$ and 3.83 when the flow approaches the cylinders at the third row, the flow has again the jet-like patterns. When we move along the cross-streamwise direction from the centerline ($y=0$) at $x=3.58$ and 3.83, the streamwise velocity has a minimum value at $y=0$, increases with increasing vertical distance due to the acceleration of flow past cylinders in the second row until it reaches the maximum value, and then decreases with further increase in the vertical distance due to flow

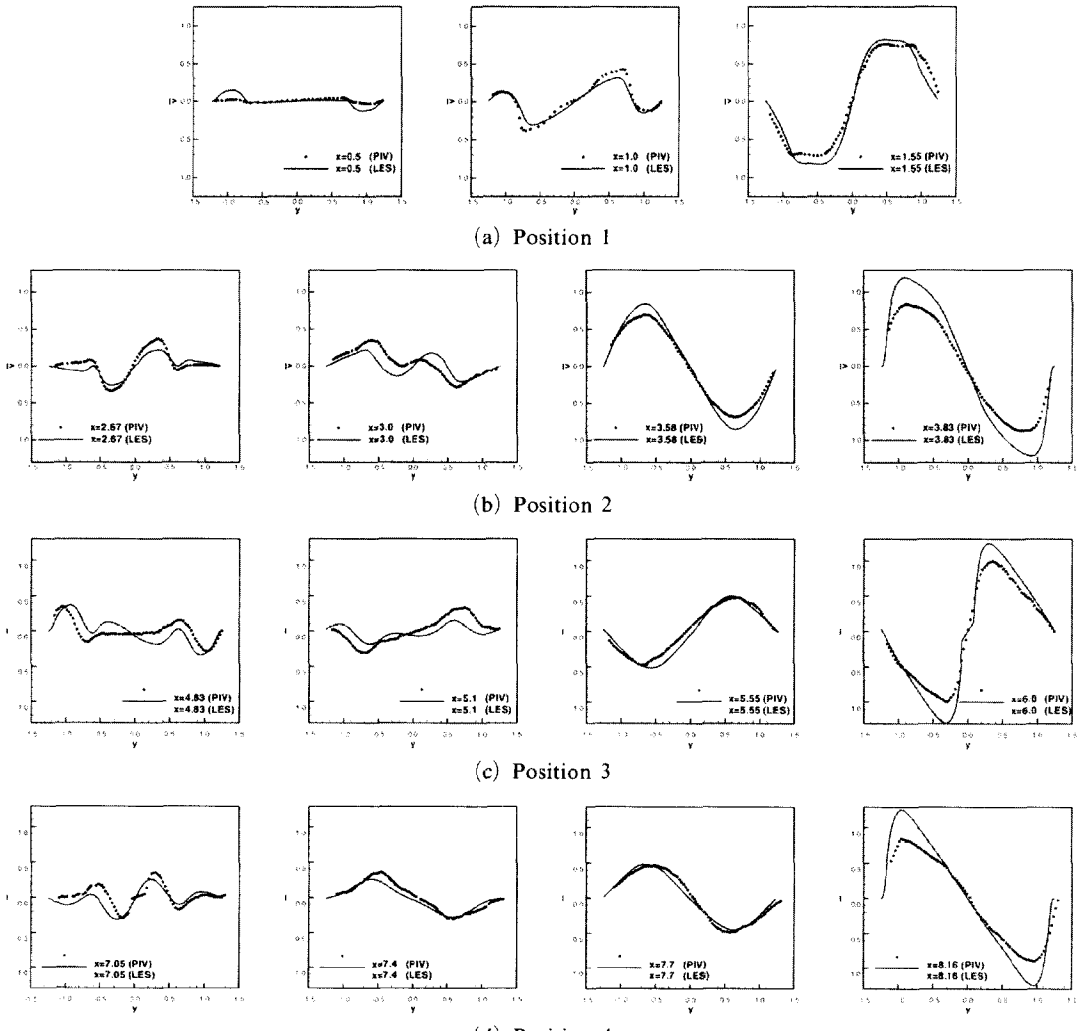

(a) Position 1

(b) Position 2

(c) Position 3

(d) Position 4

Fig. 7 Comparison of time-averaged cross-streamwise velocity obtained from the present calculation with PIV experiment: (-) this study, (▪) PIV experiment

retardation in front of cylinders in the third row. The cross-streamwise velocities at $x=3.58$ and 3.83 have a tilted "N" shape with a zero value at $y=0$ and a maximum or minimum value in between the cylinders in the cross-streamwise direction. When $y \geq 0$, the cross-streamwise velocity has a negative value due to the flow moving in the downward direction. The opposite is true when $y<0$. The flow in the position 3 changes its pattern from the wake flow after the cylinders in the third row to the jet-like flow before the cylinders in the fourth row, similar to the change in the position 1. The noticeable difference between position 1 and position 3 is an increase in the shear layer thickness and higher peak velocity in the position 3. The change in the flow pattern in the position 4 is very similar to that in the position 2. We can observe some difference in the velocity defect at $x=3.83$ and 8.16. It can be understandable that the pressure drop in the developing flow should be higher than that of the fully developed region. It can be imagined that the pressure difference between the fourth and fifth row might be much smaller than that of the

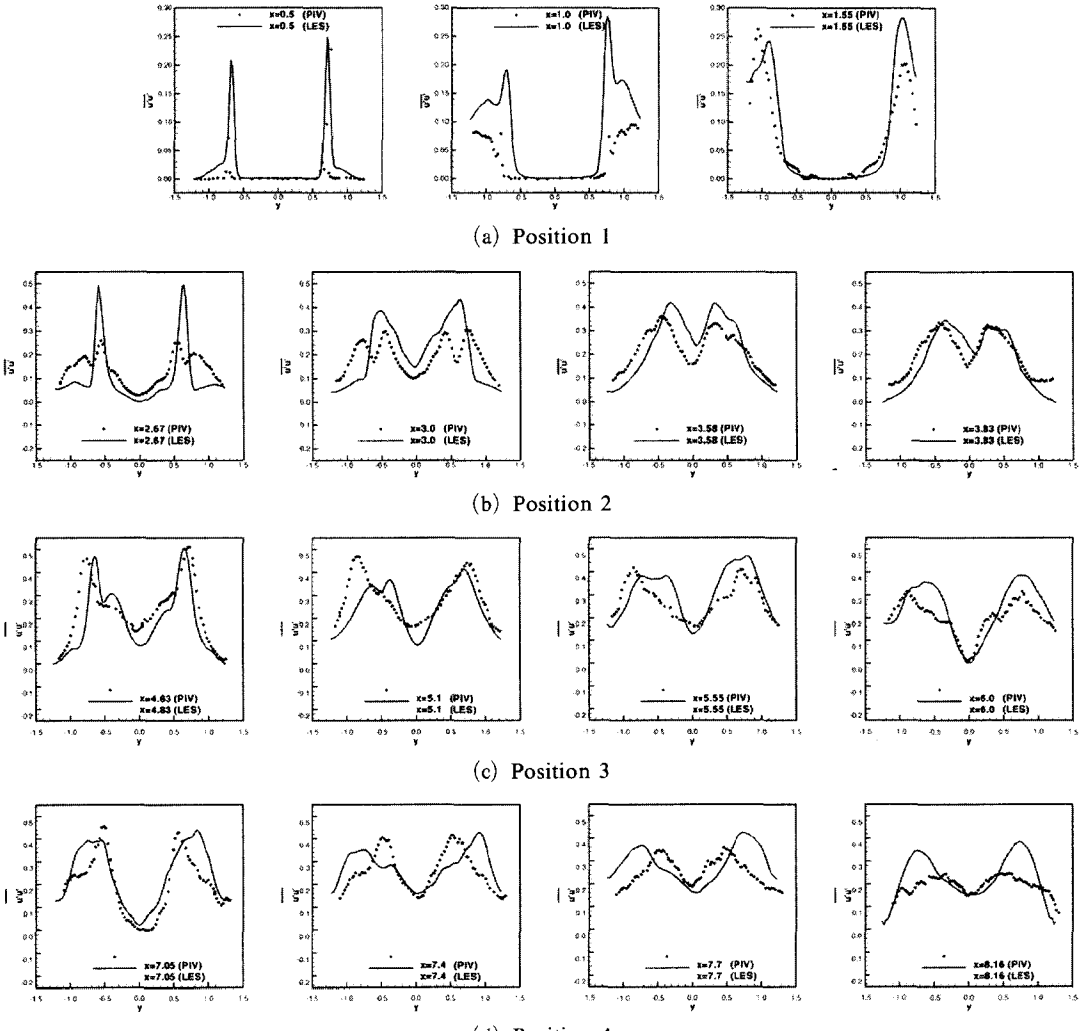

(a) Position 1

(b) Position 2

(c) Position 3

(d) Position 4

Fig. 8 Comparison of time-averaged streamwise turbulence intensity obtained from the present calculation with PIV experiment : (-) this study, (▪) PIV experiment

second and third row. Again, not much differences in the streamwise mean velocity profiles in positions 2 and 4 provide evidences that the flow could be fully developed after the fifth row. As shown in Figs. 6 and 7, the time-averaged streamwise and cross-streamwise velocities obtained from the present calculation represent generally well those obtained from the PIV experiment. However, we can observe some differences in the absolute values of streamwise and cross-streamwise velocities, because of the difference in the prediction of the recirculation length, L_F, in the wake between the computed and PIV experimental results.

Figures 8～10 show the distribution of streamwise turbulent intensitiy ($\overline{u'u'}$), cross-streamwise turbulent intensity ($\overline{v'v'}$) and Reynolds shear stress ($\overline{u'v'}$), respectively, along the cross-streamwise direction at different locations in the streamwise direction. The solid line and square symbol in these figures represent the LES calculation and PIV experimental results, respectively. In the position 1, $\overline{u'u}$, $\overline{v'v'}$ and $\overline{u'v}$ are almost zero around the centerline corresponding

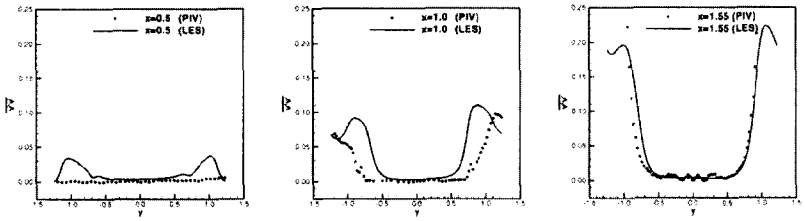

(a) Position 1

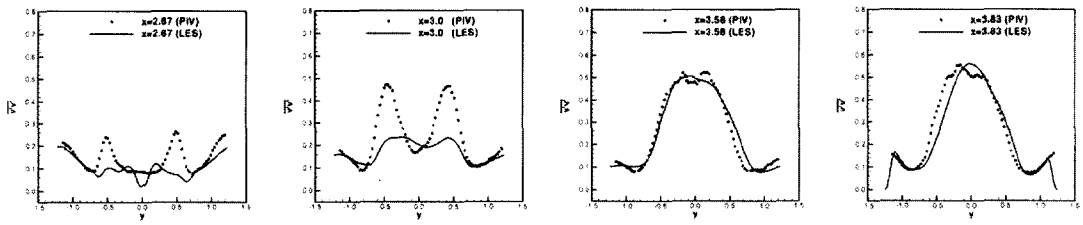

(b) Position 2

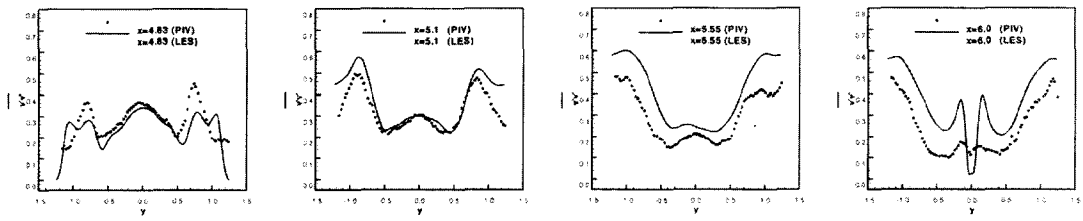

(c) Position 3

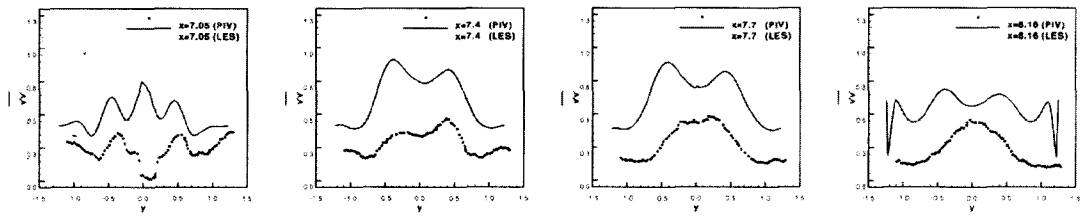

(d) Position 4

Fig. 9 Comparison of the time-averaged cross-streamwise turbulence intensity obtained from the present calculation with PIV experiment: (-) this study, (▪) PIV experiment

to the potential core region and increases when we move close to the separation bubble in the wake region. It is interesting to note that the zero shear stress line seems to coincide with the dividing streamline. Weak Reynolds shear stress is found in the back flow region behind cylinders in the first row while fairly large peak values appear at downstream of the bubble in the position 1. Zero Reynolds shear stress in the separated shear layer from the first cylinders indicates that the flow is being separated at a laminar state. Transition occurs at far downstream from the cylinder in the first row. The high velocity fluctuation in the position 1 could be the results of so-called 'pseudo turbulence', which occurs because of a periodic motion by vortex shedding.

At $x=2.67$ and 3.0 in the position 2 corresponding to the flow past cylinders in the second row, the high values of $\overline{u'u'}$, $\overline{v'v'}$ and $\overline{u'v'}$ form along the separated shear layer. It is interesting to point out that the small values of these turbulent properties are observed in the recirculation zone, which is usually quoted as 'deadwater zone'. At $x=3.58$ and 3.83 in the position 2,

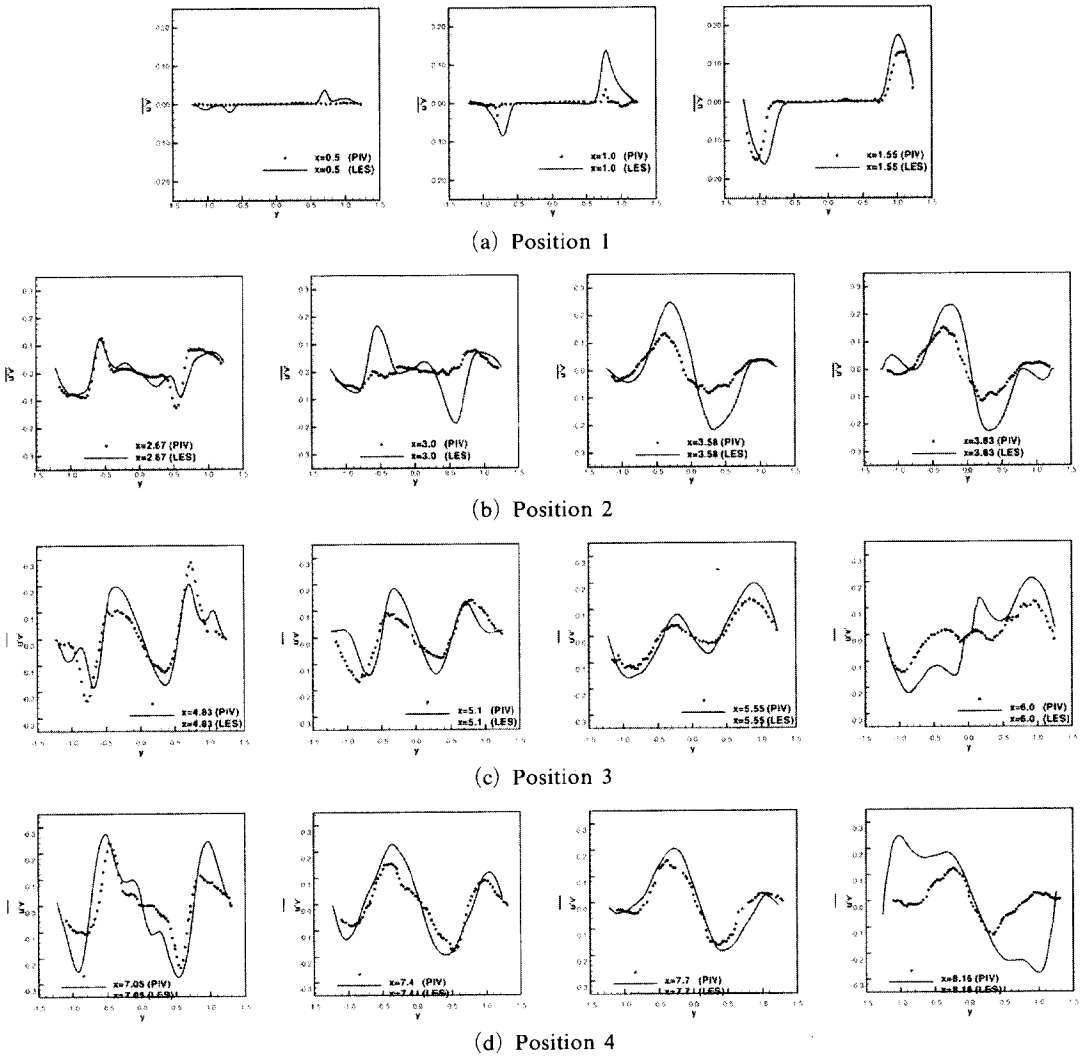

Fig. 10 Comparison of the time-averaged Reynold shear stress obtained from the present calculation with PIV experiment: (-) this study, (▪) PIV experiment

$\overline{v'v'}$ has the largest value at the centerline due to the vertical swinging motion of the jet-like structures as observed in the instantaneous velocity fields. However, $\overline{u'u'}$ and $\overline{u'v'}$ at $x=3.58$ and 3.83 have peak values along the separated shear layer in the presence of vortex shedding.

$\overline{u'u'}$, $\overline{v'v'}$ and $\overline{u'v'}$ in the position 3 have higher values along the centerline, compared to an almost zero value along the centerline in the position 1. This result shows that the flow in the position 3 is fairly high-turbulent, compared to the flow corresponding to potential core region in the position 1. $\overline{u'u'}$ in the position 3 has a low value at the centerline and peak values along the separated shear layer. $\overline{v'v'}$ at $x=4.83$ has two peak values. The peak value at the centerline seems to be caused by the vertical swinging motion of the jet-like structures. Another peak value observed at the separated shear layer might be generated by the strong interactions between the jet-like structures and the recirculating bubble. At $x=5.1$ and 5.55, the magnitude of peak value of $\overline{v'v'}$ at the centerline decreases whereas that at separated shear layer increases. At $x=6.0$, the first peak of $\overline{v'v'}$, which is located at the centerline at $x=4.83$, 5.1 and 5.55, moves slightly to upward and downward direction and is located at the place close to the centerline due to the presence of cylinder in the fourth row. At $x=4.83$, the effects of the swinging motion of the jet-like structures seem to be are larger than the interactions between the jet-like structures and the recirculating bubble, giving the larger peak values of $\overline{u'v'}$ at the place close to the centerline than the wake region. However, when we move downstream, this effect is reversed and the peak values of $\overline{u'v'}$ at the place close to the centerline become smaller than those in the wake region.

The general shape of $\overline{u'u'}$ and $\overline{u'v'}$ in the position 4 is similar to that at the position 2. The main difference is that the turbulent flow becomes much more homogeneous when we move downstream from the position 2 to the position 4. Thus we expect that the streamwise turbulent intensity and Reynolds shear stress could approach the fully developed state from the fifth rows like the bulk mean flow. However, the distribution of $\overline{v'v'}$ in the position 4 obtained from the present LES calculation is much different from that in the position 2. Thus it can be conjectured that the cross-streamwise turbulence intensities are still developing after the fifth row.

The general trend of variation in $\overline{u'u'}$ and $\overline{v'v'}$ obtained from the present LES calculation in the positions 1~4 represents well that from the PIV experiment. However we can observe some differences in the absolute magnitude between the present computed results and measured PIV data. The values of $\overline{v'v'}$ obtained from the present LES calculation in the positions 1~3 also represent generally well those from the PIV experiment, except the under-prediction of $\overline{v'v'}$ at $x=2.67$ and 3.0 which are the wake region for the flow past cylinders in the 2nd row. However, the values of $\overline{v'v'}$ obtained from the present LES calculation in the position 4 are generally higher than the PIV data. This difference of $\overline{v'v'}$ in the position 4 between the LES and PIV results can not be explained clearly at this moment. However, out-of-plane motions due to highly three-dimensional fluctuation may reduce the cross-streamwise turbulence intensities during the present PIV measurement in the position 4.

5. Conclusions

We calculated the unsteady and three-dimensional flow fields past a bank of tubes using a large eddy simulation. The developed computer code is parallelized on the basis of MPI. The computation is carried out using 24 processors.

Most of the flow region between the first and second row is a potential core. Remarkable differences in flow characteristics are observed in the region from the second row to the fourth row. Karman vortex sheddings are clearly seen in the wakes from the first and second row cylinders. However, no more periodic shedding is observed from the third row cylinders. The oscillating jet-like structure seems to be dominant from the third row. The time-averaged mean

velocity profiles and the Reynolds shear stress profiles are nearly same at both position 3 and 4, but differences in streamwise and cross-streamwise turbulent intensity are also noticeable.

We compared the time-averaged results for the mean flow and turbulent properties obtained from the present calculation with those from PIV experiments. The length of recirculation region obtained from the present calculation is slightly larger than that from the PIV experiments, resulting in the slight difference in streamwise and cross-streamwise velocities. However, the present calculation results for the time-averaged streamwise and cross-streamwise velocities represent generally well the PIV experimental data. The present calculation results for the turbulent properties also represent well the PIV data with slight difference in their absolute magnitude.

References

Ahmad, R. A., 1996, "Steady-State Numerical Solution of the Navier-Stokes and Energy Equations Around a Horizontal Cylinder at Moderate Reynolds Numbers from 100 to 500," *Heat Transfer Engineering*, Vol. 17, No. 1, pp. 31~80.

Barsamian, H. R. and Hassan, Y. A, 1997, "Large Eddy Simulation of Turbulent Cross-flow in Tube Bundles," *Nuclear Engineering and Design*, Vol. 172, pp. 103~122.

Beale, S. B. and Spalding, D. B., 1999, "A Numerical Study of Unsteady Flow in In-line and Staggered Tube Banks," *Journal of Fluids and Structure*, Vol. 13, pp. 723~754.

Braza, M., Chassaing, P. and Minh, H. H., 1986, "Numerical Study and Physical Analysis of the Pressure and Velocity Fields in the Near Wake of a Circular Cylinder," *J. Fluid Mech.*, Vol. 165, pp. 79~130.

Germano, M., Piomelli, U., Moin, P. and Cabot, W. H., 1991, "A Dynamic Subgrid-Scale Eddy Viscosity Model," *Phyics of Fluids A*, Vol. 3, pp. 1760~1765.

Ghosh Roychowdhury, D., Sarit Kumar Das and Sundararajan, T., 1999, "An Efficient Solution Method for Incompressible N-S Equations Using Non-orthogonal Collocated Grid," *Int. J. Numer. Meth. Engng*, Vol. 45, pp. 741~763.

Krishne Gowda, Y. T., Patnaik, B. S. V. P., Aswatha Narayana, P. A. and Seetharamu, K. N., 1998, "Finite Element Simulation of Transient Laminar Flow and Heat Transfer Past an In-line Bank," *International Journal of Heat and Fluid Flow*, Vol. 19, pp. 49~55.

Karniadakis, G. and Triantafyllou, G. S., 1992, "Three-Dimensional Dynamics and Transition to Turbulence in the Wake of Bluff Objects," *J. Fluid Mech.*, Vol. 238, pp. 1~30.

Kim, J. G., 2002, "Direct Numerical Simulation of Natural Convection in Internally Finned Annulus Using Parallel Implementation," M.S. Thesis, Pusan National University, Pusan, Korea.

Kravchenko, A. G. and Moin, P., 2000, "Numerical Studies of Flow over a Circular Cylinder at Re_D=3900," *Physics of Fluids*, Vol. 12, No. 2, pp. 403~417.

Lourenco, L. M. and Shih, C., "Characteristics of the Plane Turbulent Near Wake of a Circular Cylinder. A Particle Image Velocimetry Study," *private communication.*

Manson, P. J. and Callen, N. S., 1986, "On the Magnitude of the Subgrid-Scale Eddy Coefficient in Large Eddy Simulations of Turbulent Channel Flow," *J. Fluid Mech.*, Vol. 162, pp. 439~462.

Mittal, R. and Balachandar, S., 1994, "Direct Numerical Simulation of Flow Past Elliptic Cylinders," *Journal of Computational Physics*, Vol. 124, pp. 351~367.

Mittal, R. and Balachandar, S., 1995, "Generation of Streamwise Vortical Structures in Bluff Body Wakes," *Phys. Review Letters*, Vol. 75, No. 8, pp. 1300~1302.

Park, J. D., 2001, "Measurement of Flow Field in a Staggered Tube Bundle Using Particle Image Velocimetry," M.S. Thesis, Pusan National University, Pusan, Korea.

Patankar, S. V., 1980, *Numerical Heat Transfer and Fluid Flow*. Hemisphere/McGraw-Hill, Washington, pp. 113~135.

Ryu, B., Kim, K. and Boo. J., 2003, "The Effect of Serrated Fins on the Flow Around a Circular Cylinder," *KSME International J.*, Vol. 17, No. 6, pp. 925~934.

Tamura, T. and Ohta, I., 1990, "On the Reliability of Two-dimensional Simulation for Unsteady Flows Around a Circular-type Structure," *J. Wind Eng. and Industrial Aero.*, Vol. 35, pp. 275~298.

Thompson, M., Hourigan, K. and Sheridan, J., 1996, "Three-Dimensional Instabilities in the Wake of a Circular Cylinder," *Experimental Thermal and Fluid Science*, Vol. 12, pp. 190~196.

Wang, Y. Q., Penner, L. A. and Ormiston, S. J., 2000, "Analysis of Laminar Forced Convection of Air for Crossflow in Banks of Staggered Tubes," *Numerical Heat Transfer, Part A*, Vol. 38, pp. 819~845.

Watterson, J. K., Dawes, W. N., Savil, A. M. and White, A. J., 1999, "Predicting Turbulent Flow in a Staggered Tube Bundle," *International Journal of Heat and Fluid Flow*, Vol. 20, pp. 581~591.

Williamson, C. H. K., 1996a, "Three-Dimensional Wake Transition," *J. Fluid Mech.*, Vol. 328, pp. 345~407.

Williamson, C. H. K., 1996b, "Vortex Dynamics in the Cylinder Wake," *Annu. Rev. Fluid Mech.*, Vol. 28, pp. 477~543.

Wilson, A. S. and Bassiouny, M. K., 2000. "Modeling of Heat Transfer for Flow Across Tube Banks," *Chemical Engineering and Processing*, Vol. 39, pp. 1~14.

Yoo, S., Park, D. and Chung, M., 2002, "Heat Transfer Enhancement for Fin-Tube Heat Excganger Using Vortex Generators," *KSME International J.*, Vol. 16, No. 1, pp. 109~115.

Yoon, S. Y., 2000, "PIV Measurements in the Turbulent Near Wake of a Circular Cylinder," M.S. Thesis, Pusan National University, Pusan, Korea.

Zhang, J. and Dalton, C., 1998, "A Three-dimensional Simulation of a Steady Approach Flow Past a Circular Cylinder at Low Reynolds Number," *Int. J. Numer. Meth. Fluids*, Vol. 26, pp. 1003~1022.